

Global response of floods to tropical explosive volcanic eruptions

Received: 30 October 2024

Accepted: 28 July 2025

Published online: 26 August 2025

 Check for updates

Hanbeen Kim^{1,2}, Gabriele Villarini^{1,2}✉, Wenchang Yang^{1,3} & Gabriel Vecchi^{1,2,3}

Tropical volcanic eruptions with a high volcanic explosivity index (≥ 5) impact the global climate system, but little is known about how they affect floods. Here, leveraging global climate model simulations with volcanic forcings and statistical relationships between seasonal climate drivers and peak discharge, we investigate the response of seasonal peak discharges at 7,886 streamgauges worldwide to three tropical explosive volcanic eruptions in the twentieth century: Agung 1963 (Indonesia), Santa Maria 1902 (Guatemala) and Pinatubo 1991 (Philippines), whose stratospheric aerosol plumes were distributed primarily in the Southern Hemisphere, primarily in the Northern Hemisphere and symmetrically across both hemispheres, respectively. For the eruptions with interhemispherically asymmetric aerosol distributions, tropical regions show more immediate and widespread responses to the eruptions than non-tropical regions, with a distinct interhemispheric contrast of decreasing (increasing) peak discharges in the hemisphere in which the eruption happened (did not happen). For the case of symmetric aerosol distribution, tropical (arid) regions have the strongest tendency to respond to the eruption by decreasing (increasing) peak discharges in both hemispheres. These regional flood responses are attributed mainly to seasonal precipitation changes across the climate regions. Beyond direct volcanic hazards, our study provides a global view of the secondary flood hazards resulting from hydroclimatic changes induced by large explosive eruptions.

Flooding is one of the most destructive and widespread natural disasters globally, affecting millions of people annually and causing substantial economic losses¹. Although this hazard is generated by a complex interplay of topographic, anthropogenic and meteorological factors, the primary drivers that control the magnitudes of floods globally are precipitation and temperature as proxies for different physical processes (for example, direct runoff, antecedent wetness, snow accumulation and melt)^{2–5}. Therefore, temporary but abrupt climate perturbations induced by natural disturbances (for example, solar variability and volcanic eruption) can affect flooding by causing transient modifications in precipitation and temperature⁶.

Tropical explosive volcanic eruptions impact the global climate by releasing massive amounts of sulfur dioxide gas into the stratosphere, where it is then oxidized to form sulfate aerosols that spread through stratospheric circulation. These aerosols scatter incoming solar radiation and absorb outgoing terrestrial radiation, leading to surface and tropospheric cooling and stratospheric warming (a phenomenon referred to as volcanic forcing), which in turn affects atmospheric circulation. Many studies have examined the impact of tropical volcanic eruptions on global climate phenomena (for example, El Niño–Southern Oscillation, North Atlantic Oscillation and monsoon circulation) and climate variables (for example, precipitation and

¹Department of Civil and Environmental Engineering, Princeton University, Princeton, NJ, USA. ²High Meadows Environmental Institute, Princeton University, Princeton, NJ, USA. ³Department of Geosciences, Princeton University, Princeton, NJ, USA. ✉e-mail: gvillari@princeton.edu

temperature)^{7–10}. Meanwhile, even though some limited studies have focused on the responses of surface runoff and streamflow at regional or global scales^{11–14}, little is known about the global responses of floods to volcanism.

To better constrain the connection between flooding and volcanic eruptions, we utilize a modelled statistical relationship between observed seasonal peak flows and their climate drivers—namely, basin- and season-averaged precipitation and temperature—at each of the 7,886 streamgauges worldwide. These seasonal climate drivers serve as effective proxies of primary factors in flood generation (for example, heavy precipitation and antecedent wetness conditions) under various climate regions and catchment processes worldwide^{2,15} (Extended Data Fig. 1). When evaluating the model's predictive performance across four climate types (tropical, arid, temperate and cold) and seasons, the seasonal statistical flood models performed well overall, with a median correlation coefficient between observed and modelled peak flows exceeding 0.53, regardless of season or climate type (Extended Data Fig. 1). Therefore, this statistical flood model allows us to investigate the response of seasonal peak discharges to volcanic eruptions by using seasonal precipitation and temperature derived from climate model simulations with volcanic forcings as inputs (Methods).

Previous studies demonstrated that hydroclimatic responses to volcanic eruptions exhibit distinct hemispheric differences depending on radiative forcing structures (interhemispheric asymmetry and symmetry)^{16–18}. Here, we focus on three tropical explosive volcanic eruptions in the twentieth century, each representing a different case of interhemispherically symmetric or asymmetric aerosol distribution with the highest volcanic explosivity index (VEI)¹⁹: the 1963 eruption of Agung in Indonesia, Southeast Asia (VEI of 5 with aerosol plumes mostly in the Southern Hemisphere (SH)), the 1902 eruption of Santa Maria in Guatemala, Central America (VEI of 6 with aerosol plumes mostly in the northern hemisphere (NH)) and the 1991 eruption of Pinatubo in Philippines, Southeast Asia (VEI of 6 with a more symmetric aerosol distribution between the two hemispheres). We use ensemble outputs simulated from the Forecast-oriented Low Ocean Resolution (FLOR) model, which is a fully coupled global climate model extensively used to simulate and predict hydroclimatic responses to various climate conditions. By forcing the statistical flood model with seasonal precipitation and temperature simulated from the three volcanic eruptions and non-eruption (that is, baseline simulation) (Methods), we examine the prevalence and magnitude of changes in peak discharges with and without volcanic eruptions at the global scale (Extended Data Fig. 1).

Temporal changes in prevalence of global flood responses

For each of 7,886 streamgauges across the globe, we examine if there are significant changes in the 2-year return interval (RI) discharges between eruption and non-eruption simulations on a seasonal basis. We then assess how the proportion of streamgauges with this response changes over time for each hemisphere. In the case of the Agung eruption, whose plume distribution is more concentrated towards the SH, the response of the 2-year RI discharges exhibits opposing temporal patterns between the two hemispheres (Fig. 1). Across the whole SH, the percentage of streamgauges where the eruption reduces peak discharges increases abruptly by ~25% during the first year after the eruption and then gradually declines, while the signal of increasing changes is more muted and less than ~10%. By contrast, the NH shows the opposite temporal pattern: the percentage of streamgauges with decreasing changes is limited to less than 12%, while that with an increase in peak flow due to the eruption gradually increases by ~20% during the third year after the eruption, before declining.

To further examine the volcanic impact on 2-year RI discharges, we stratify these results by climate region into tropical, arid, temperate and cold regions (Fig. 1). The tropical region is the most affected by the eruption, showing decreasing changes in 2-year RI discharges

at half of the SH streamgauges in the first year, and it remains the most affected by the eruption into the fourth year after the event. The arid and temperate regions exhibit a similar temporal pattern, but with smaller percentages overall. In the NH, the tropical region is also the most affected during the overall period, experiencing a sharp rise to ~40% in the percentage of streamgauges with increasing peak flows in the first year, followed by a gradual decrease, despite marked seasonal variation. This temporal pattern is different from the other climate regions in the NH, where the impact of Agung gradually increases up to the third year after the eruption.

In the case of the Santa Maria eruption, which has an aerosol distribution more concentrated in the NH, there is also a more distinct volcanic impact on 2-year RI discharges when breaking down the results by climate regions (Fig. 1). In both hemispheres, compared with other climate regions, the impact of the eruption is more pronounced in the tropics during the first 2 years after the eruption, with an abrupt increase in the percentage of sites experiencing increased flows to ~24% in the SH and decreased flows to ~35% in the NH. These results indicate that tropical regions respond more rapidly and prevalently than other climate regions to tropical volcanic eruptions with interhemispherically asymmetric plumes, showing predominant decreases in peak flows in the hemisphere with higher aerosol concentrations and increases in the hemisphere with lower concentrations. Meanwhile, arid and temperate regions in the NH are more susceptible to increased peak flows due to the Santa Maria eruption, with an increase to ~23% in the percentage of sites having increased flow in the first 2 years after the eruption. These results indicate that the impact of tropical volcanic eruptions on seasonal peak discharges can vary among climate regions.

When analysing the more globally widespread (that is, interhemispherically symmetric) aerosol plume from the Pinatubo eruption, we also observe differences in both the direction and magnitude of volcanic impacts on 2-year RI discharges across climate regions (Fig. 1). The effect of the Pinatubo eruption in reducing peak flows is prominent in the tropical region, with an increase of up to ~21% and ~34% in the percentage of corresponding streamgauges by the second year after the eruption in the SH and NH, respectively. By contrast, arid regions are the most affected by the eruption in terms of increasing peak flows, with an increase of up to ~36% in the percentage of corresponding streamgauges by the third year after the eruption in both NH and SH. The effect of the Pinatubo eruption in increasing peak flows is also found in other climate regions in the NH, with an increase of up to ~30%, ~25% and ~25% in the percentage of temperate, cold and tropical streamgauges, respectively.

We explore the geographical distribution of the streamgauges where peak flows respond significantly to eruptions, focusing on the season with the most pronounced flood response (Fig. 2). For the September–November (SON) season of the first Agung eruption year, southeastern Brazil accounts for the majority of the 2-year RI discharge reduction in the SH tropical regions, while western Africa and the Indian subcontinent account for most of the 2-year RI discharge increase in the NH tropical regions. The prevalence of flood response in these regions diminishes over time. For the Santa Maria eruption, December–February (DJF) peak flow reductions in the NH during the first year are seen mainly over the Indian subcontinent and North America. In the second year, the reduction response is more prevalent in Western Europe, composed mainly of temperate and cold regions. By the third year, these regional concentrations disperse. When looking at the March–May (MAM) seasonal response of the Pinatubo eruption, the southwestern, southeastern and northeastern USA account for most of the peak flow increase in the NH arid, temperate and cold regions, respectively, during the first 2 years. Meanwhile, southeastern Brazil and South Africa contribute most to the peak flow increase in the peak flow of the SH tropical and arid regions, respectively, over the first 3 years from the eruption. This spatial analysis suggests that

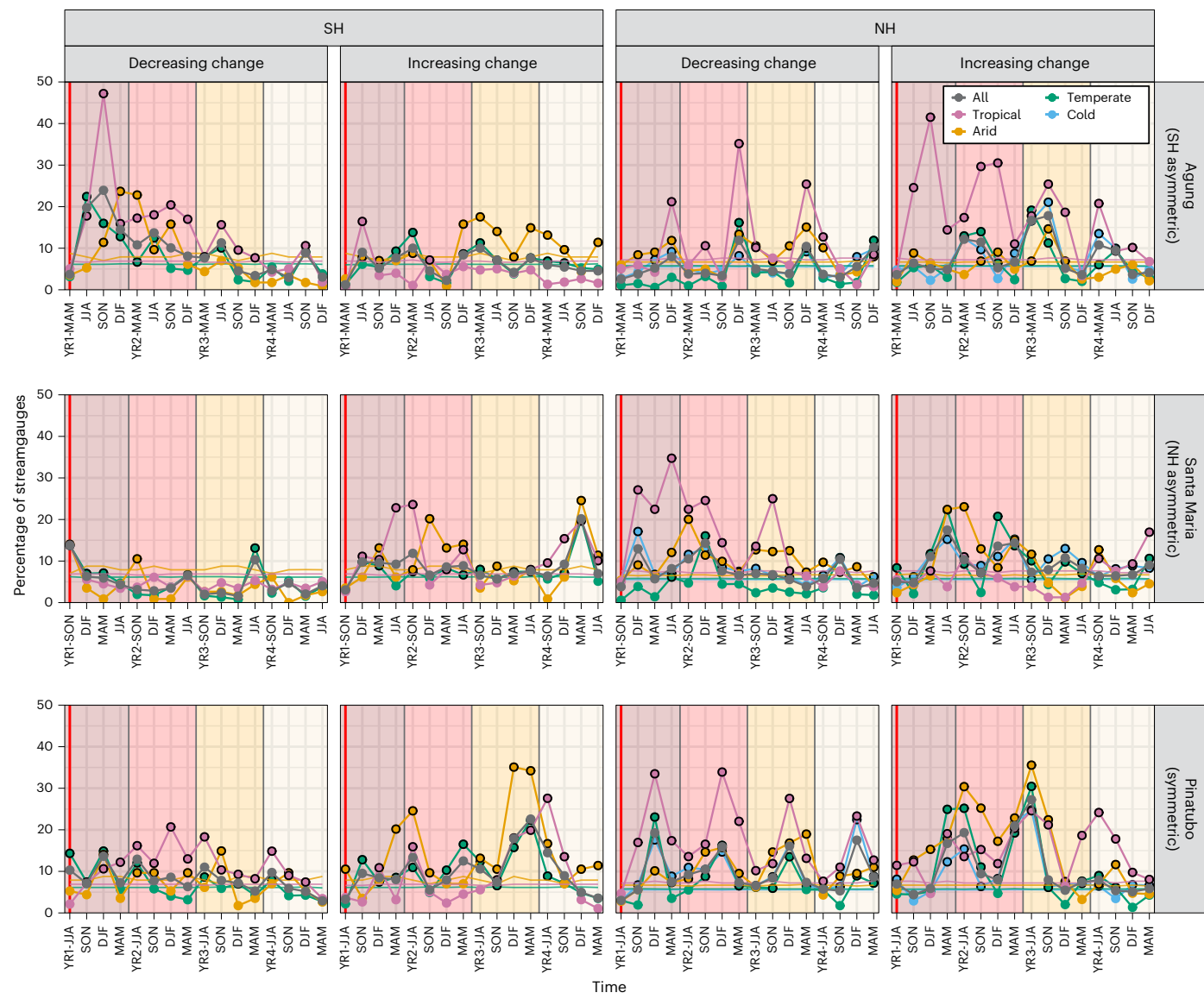


Fig. 1 | Changes over time in the prevalence of the 2-year RI discharges in response to tropical volcanic eruptions. Percentages of streamgauges showing significant decreases (first and third columns) and increases (second and fourth columns) in the 2-year RI discharges calculated for the entire hemispheric (black line with points), tropical (magenta line with points), arid (orange line with points), temperate (green line with points) and cold (light-blue line with points) regions. Solid horizontal lines represent threshold percentages of streamgauges

showing significant changes not due to chance at the 5% significance level, and points above these lines are highlighted with a black border. The vertical red line indicates the season in which the eruption occurred. The shaded areas separated by different colours and vertical black lines represent each year, from the first (YR1) to the fourth year (YR4) after the eruption. Panels show results for Agung (Indonesia), Santa Maria (Guatemala) and Pinatubo (Philippines) eruptions.

global flood responses to tropical volcanic eruptions can vary geographically over time.

The aforementioned results pertain to the 7,886 globally available streamgauges, without accounting for overlapping basins or spatial density. To assess the impact of overlapping basins, we conduct the same analysis for 4,886 streamgauges with non-overlapping basins (Extended Data Fig. 2; Methods). The results show no marked difference between all 7,886 streamgauges and the subset with non-overlapping basins, with nearly identical temporal patterns (Extended Data Fig. 3). Furthermore, we examine the sensitivity of our results to the performance of the statistical flood model (Extended Data Fig. 4). As we consider streamgauges with better model performance, the number of available streamgauges declines, which results in greater seasonal variation in the results. Nonetheless, the results exhibit similar temporal patterns to those for all 7,886 streamgauges, indicating that neither overlapping basins nor the statistical flood model performance distort our findings.

Seasonality of changes in global flood magnitudes

We broaden our understanding by examining how much peak flows change in response to the tropical volcanic eruptions (Fig. 3). In tropical regions, the relative changes in the 2-year RI discharge magnitudes under all hemispheric forcings increased by 2.8–17.6% for streamgauges that experience discharge increases, while discharge magnitudes diminished by -2.1% to -11.6% at those streamgauges that experience a decline in discharge. Temperate and cold regions exhibit slightly larger relative changes in discharge magnitude compared to the tropics, with increases ranging from 3.6% to 28.3% and decreases ranging from -3.8% to -13.2% for streamgauges with increased and decreased peak flows, respectively. Arid regions are overall the most sensitive to the eruptions, particularly during the DJF and MAM seasons in the SH, with relative changes in discharge magnitudes ranging from 17.2% to 65.6% for streamgauges with increased peak flows and from -6.4% to -38.2% for those with decreased peak flows. However, the picture is different if we analyse the results in terms of absolute changes in discharge

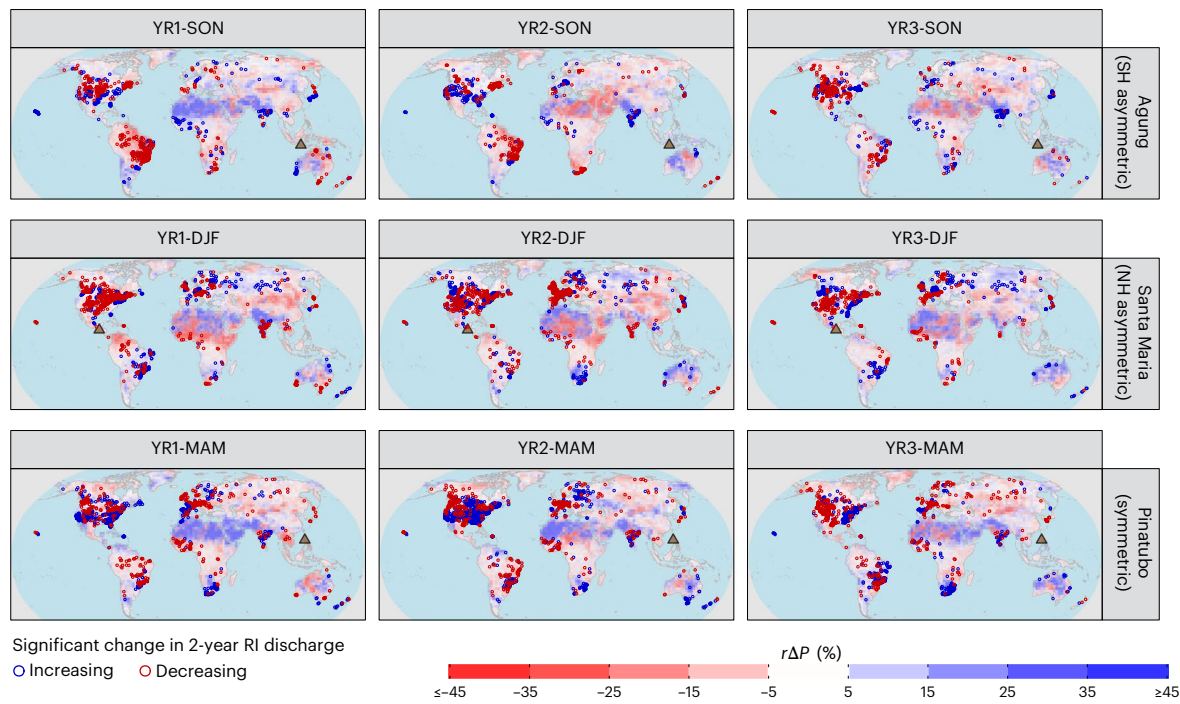


Fig. 2 | Global responses of the 2-year RI discharges and seasonal precipitation to tropical volcanic eruptions. The red (blue) circles show the streamgauges having statistically significant decreases (increases) in the 2-year RI discharge due to the eruptions. Grid cells inland indicate relative changes in the median of the season-averaged precipitation across 30 ensemble members. The redder grids represent greater decreases, while the bluer grids represent greater

increases in precipitation due to the eruptions. Three rows represent the results for SON for Agung (Indonesia), DJF season for Santa Maria (Guatemala) and MAM season for Pinatubo (Philippines) eruptions, from top to bottom. The three columns represent the results of the first (YR1), second (YR2) and third year (YR3) after the eruptions, from left to right.

magnitudes (Extended Data Fig. 5). In the SH, tropical and arid regions show distinct seasonal patterns, with greater increases and decreases in the 2-year RI discharge magnitudes during the DJF and MAM seasons. Given that DJF and MAM are the wet seasons for tropical and arid regions in the SH², this result indicates that volcanic eruptions can both mitigate and intensify discharge magnitudes, resulting in regional imbalances in the flood hazard. This is also true in the NH, where the wet seasons of tropical and arid regions are June–August (JJA) and SON, and MAM and JJA, respectively. Compared with tropical and arid regions, temperate and cold regions exhibit much less seasonal variation in discharge magnitude changes (Extended Data Fig. 5).

Physical mechanisms leading to flood responses

Although tropical explosive volcanic eruptions are known to reduce global mean precipitation^{13,20}, eruptions with aerosol concentrations predominantly over one hemisphere can produce asymmetric precipitation responses between the hemispheres, especially in global monsoon regions^{12,16,17}. For example, precipitation in one hemisphere can be increased by volcanic forcing in the other hemisphere, owing to cross-equatorial flow changes and the meridional shift of the Intertropical Convergence Zone (ITCZ)^{12,17,18,21,22}. The cross-equatorial flow from one hemisphere, resulting from enhanced hemispheric thermal contrast by the volcanic forcing, transports moist air into the monsoon regions and enhances precipitation of the opposite hemisphere. Also, enhanced thermal contrast between hemispheres moves the ITCZ away from the hemisphere experiencing volcanic impact, resulting in more precipitation in the opposite hemisphere. The simulations of the Agung and Santa Maria eruptions with an asymmetric aerosol forcing show this hemispherically asymmetric behaviour in precipitation, especially in low latitudes (Fig. 2 and Supplementary Figs. 1–4). Because precipitation exhibits a clearer positive relationship with peak flow compared with temperature (compare Fig. 2 and Supplementary Figs. 1–4 with Extended Data Fig. 6 and Supplementary Figs. 5–8),

precipitation changes driven by these mechanisms lead to interhemispheric contrast of the response of seasonal peak flows to the Agung and Santa Maria eruptions, although the temporal pattern and the degree of these responses vary depending on climate regions (Fig. 2).

For the case with asymmetric forcings, the tropical region shows the most widespread responses to eruptions in both hemispheres, with a sharp increase in the percentage of streamgauges that showed a significant change within the first year after an eruption (Fig. 1). Because the range of ITCZ shifts due to volcanic eruptions is typically limited to low latitudes, with movement maximized within the first year after the eruption and gradually returning to its preeruption conditions over several years²³, the migration of the ITCZ may be the main physical mechanism of changes in seasonal peak flows in the tropical region in response to the eruptions with asymmetric aerosol distributions. Meanwhile, other climatic regions (that is, arid, temperate and cold) mostly located far from the Equator exhibit relatively weak and/or gradual response of peak flows to the eruptions, indicating that these results may be caused by other mechanisms due to general cooling (Extended Data Fig. 6) (for example, saturation vapour pressure reduction and other atmospheric circulation changes) rather than by the impact of the changes in cross-equatorial flow and ITCZ.

For Pinatubo with interhemispherically symmetric forcing, the peak flow reduction is most evident in the tropical regions of both hemispheres and is more pronounced in the NH than in the SH (Fig. 1). Meanwhile, the peak flow increase is most noticeable in the arid regions of both hemispheres, particularly in the first 3 years after an eruption. The shift towards increased peak discharge in arid regions is consistent with previous studies¹⁴, which show that global arid regions tend to become wetter following volcanic eruptions—regardless of the hemisphere in which the forcing occurs—primarily due to the monsoon–desert coupling mechanism²⁴. Tropical explosive eruptions induce a secondary atmospheric circulation through the monsoon–desert mechanism, with descending motion over the Asian monsoon

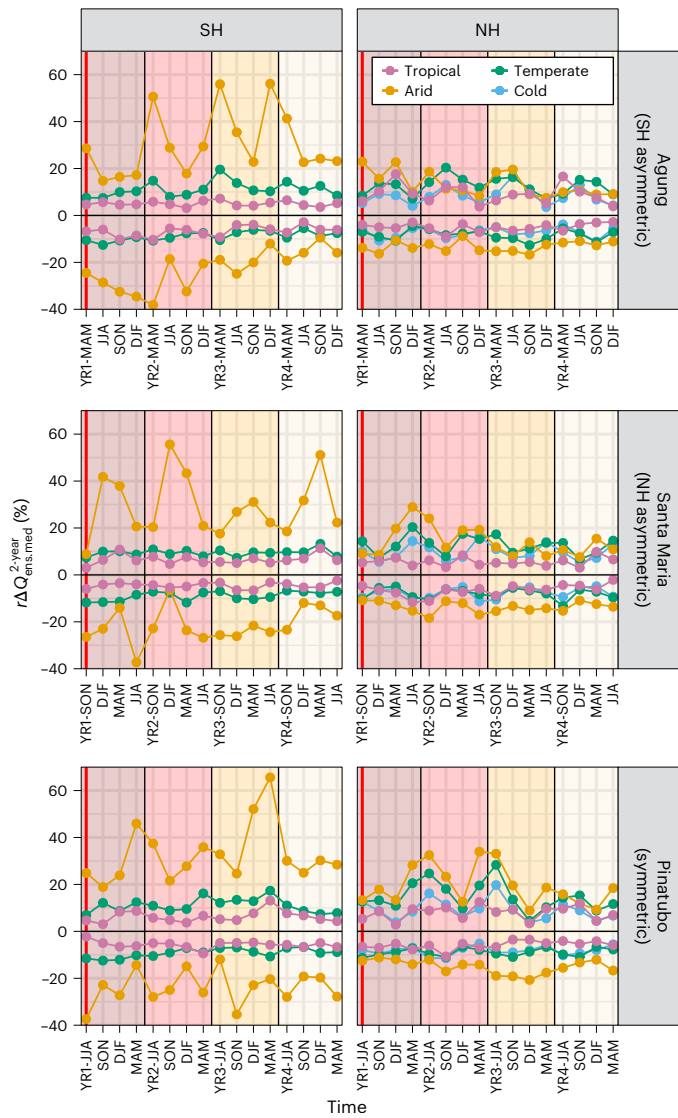


Fig. 3 | Changes over time in the regional average of the relative changes in the magnitude of the 2-year RI discharges in response to tropical volcanic eruptions. Changes in the discharge magnitude due to the eruptions calculated by subtracting the ensemble median of 30 non-eruption simulations from that of 30 eruption simulations. The regional average values are obtained by taking the median across the streamgauges stratified by tropical (magenta line), arid (orange line), temperate (green line) and cold (light-blue line) regions. The lines above (below) zero show the results for streamgauges experiencing increasing (decreasing) discharge due to the eruptions. The vertical red line indicates the season in which the eruption occurred. The shaded areas separated by different colours and vertical black lines represent each year, from the first (YR1) to the fourth year (YR4) after the eruption. Panels show results for Agung (Indonesia), Santa Maria (Guatemala) and Pinatubo (Philippines) eruptions.

region and ascending motion over the neighbouring arid regions¹⁴. This updraft causes anomalous advection of vertical moisture, resulting in increased precipitation in global arid regions.

While the direct influences of volcanic eruptions on streamflow and peak discharge by altering basin hydrology (for example, shifts in river morphology and reduction of vegetation and infiltration rate) are limited to neighbouring areas^{25,26}, massive amounts of sulfur-rich gases emitted during eruptions can disturb global hydrologic responses by changing atmospheric circulation and reducing saturation vapour pressure in accordance with the Clausius–Clapeyron relationship. We show that volcanic eruptions can lead to significant responses of the 2-year RI discharges through such teleconnections. Although global

mean rainfall and temperature decrease after volcanic eruptions, the direction and prevalence of the 2-year RI discharge responses vary depending on radiative forcing structure (that is, interhemispheric symmetry), with tropical regions being the most sensitive (that is, prevalent, intense and immediate). Furthermore, for rarer floods (that is, floods with longer RI), a greater (or smaller) number of streamgauges exhibit a significant increase (or decrease) in discharge magnitude in response to a volcanic eruption, particularly in the NH (Extended Data Fig. 7). This result suggests that if a more severe flood occurs during the period following a volcanic eruption, it may cause greater damage across more basins compared with volcanically quiescent periods. Findings from this work highlight the need to assess the impact of future volcanic eruptions not only in terms of their direct hazards (for example, lava flows, pyroclastic flows and tephra fall) but also in terms of secondary flood responses worldwide.

Online content

Any methods, additional references, Nature Portfolio reporting summaries, source data, extended data, supplementary information, acknowledgements, peer review information; details of author contributions and competing interests; and statements of data and code availability are available at <https://doi.org/10.1038/s41561-025-01782-5>.

References

1. *Human Cost of Disasters: An Overview of the Last 20 Years (2000–2019)* (CRED & UNDRR, 2020); <https://www.undrr.org/publication/human-cost-disasters-overview-last-20-years-2000-2019>
2. Kim, H., Villarini, G., Wasko, C. & Tramblay, Y. Changes in the climate system dominate inter-annual variability in flooding across the globe. *Geophys. Res. Lett.* **51**, e2023GL107480 (2024).
3. Wasko, C., Nathan, R. & Peel, M. C. Changes in antecedent soil moisture modulate flood seasonality in a changing climate. *Water Resour. Res.* **56**, e2019WR026300 (2020).
4. He, W., Kim, S., Wasko, C. & Sharma, A. A global assessment of change in flood volume with surface air temperature. *Adv. Water Resour.* **165**, 104241 (2022).
5. Stewart, I. T. Changes in snowpack and snowmelt runoff for key mountain regions. *Hydrol. Process.* **23**, 78–94 (2009).
6. Overpeck, J. T. & Cole, J. E. Abrupt change in Earth's climate system. *Annu. Rev. Environ. Resour.* **31**, 1–31 (2006).
7. Shindell, D. T., Schmidt, G. A., Mann, M. E. & Faluvegi, G. Dynamic winter climate response to large tropical volcanic eruptions since 1600. *J. Geophys. Res.* **109**, D05104 (2004).
8. Timmreck, C. et al. Linearity of the climate response to increasingly strong tropical volcanic eruptions in a large ensemble framework. *J. Clim.* **37**, 2455–2470 (2024).
9. Hermanson, L. et al. Robust multiyear climate impacts of volcanic eruptions in decadal prediction systems. *J. Geophys. Res. Atmos.* **125**, e2019JD031739 (2020).
10. Tejedor, E., Steiger, N. J., Smerdon, J. E., Serrano-Notivoli, R. & Vuille, M. Global hydroclimatic response to tropical volcanic eruptions over the last millennium. *Proc. Natl Acad. Sci. USA* **118**, e2019145118 (2021).
11. Iles, C. E. & Hegerl, G. C. Systematic change in global patterns of streamflow following volcanic eruptions. *Nat. Geosci.* **8**, 838–842 (2015).
12. Zuo, M., Zhou, T. & Man, W. Hydroclimate responses over global monsoon regions following volcanic eruptions at different latitudes. *J. Clim.* **32**, 4367–4385 (2019).
13. Trenberth, K. E. & Dai, A. Effects of Mount Pinatubo volcanic eruption on the hydrological cycle as an analog of geoengineering. *Geophys. Res. Lett.* **34**, 1–5 (2007).
14. Zuo, M., Zhou, T. & Man, W. Wetter global arid regions driven by volcanic eruptions. *J. Geophys. Res. Atmos.* **124**, 13648–13662 (2019).

15. Liu, J. et al. Global changes in floods and their drivers. *J. Hydrol.* **614**, 128553 (2022).
16. Yang, W. et al. Climate impacts from large volcanic eruptions in a high-resolution climate model: the importance of forcing structure. *Geophys. Res. Lett.* **46**, 7690–7699 (2019).
17. Liu, F. et al. Global monsoon precipitation responses to large volcanic eruptions. *Sci. Rep.* **6**, 24331 (2016).
18. Colose, C. M., LeGrande, A. N. & Vuille, M. Hemispherically asymmetric volcanic forcing of tropical hydroclimate during the last millennium. *Earth Syst. Dyn.* **7**, 681–696 (2016).
19. Robock, A. in *The Encyclopedia of Volcanoes* (ed. Sigurdsson, H.) 935–942 (Academic, 2015); <https://doi.org/10.1016/B978-0-12-385938-9.00053-5>
20. Iles, C. E., Hegerl, G. C., Schurer, A. P. & Zhang, X. The effect of volcanic eruptions on global precipitation. *J. Geophys. Res. Atmos.* **118**, 8770–8786 (2013).
21. Zhuo, Z., Kirchner, I., Pfahl, S. & Cubasch, U. Climate impact of volcanic eruptions: the sensitivity to eruption season and latitude in MPI-ESM ensemble experiments. *Atmos. Chem. Phys.* **21**, 13425–13442 (2021).
22. Iles, C. E. & Hegerl, G. C. The global precipitation response to volcanic eruptions in the CMIP5 models. *Environ. Res. Lett.* **9**, 104012 (2014).
23. Erez, M. & Adam, O. Energetic constraints on the time-dependent response of the ITCZ to volcanic eruptions. *J. Clim.* **34**, 9989–10006 (2021).
24. Rodwell, M. J. & Hoskins, B. J. Monsoons and the dynamics of deserts. *Q. J. R. Meteorol. Soc.* **122**, 1385–1404 (1996).
25. Pierson, T. C. & Major, J. J. Hydrogeomorphic effects of explosive volcanic eruptions on drainage basins. *Annu. Rev. Earth Planet. Sci.* **42**, 469–507 (2014).
26. Todesco, M. & Todini, E. Volcanic eruption induced floods. a rainfall-runoff model applied to the Vesuvian Region (Italy). *Nat. Hazards* **33**, 223–245 (2004).

Publisher's note Springer Nature remains neutral with regard to jurisdictional claims in published maps and institutional affiliations.

Springer Nature or its licensor (e.g. a society or other partner) holds exclusive rights to this article under a publishing agreement with the author(s) or other rightsholder(s); author self-archiving of the accepted manuscript version of this article is solely governed by the terms of such publishing agreement and applicable law.

© The Author(s), under exclusive licence to Springer Nature Limited 2025

Methods

Climate drivers simulated from three tropical volcanic eruptions and a non-eruption scenario

We use the FLOR model to simulate global climate with high horizontal resolution (~50 km) from three tropical volcanic eruptions, each representing an interhemispherically different case of aerosol plume distribution. The Agung (Indonesia) and Santa María (Guatemala) eruptions had more concentrated SO₂ aerosols over the SH and NH, respectively, whereas the SO₂ aerosol plume in the Pinatubo (Philippines) eruption was dispersed across both hemispheres. Through a pre-industrial control (piControl) simulation generally used as a baseline for detecting external forcings, we first obtained ensemble outputs for 5 years based on 30 different initial conditions randomly selected from the simulated global climate in equilibrium from the PiControl run. For tropical volcanic simulations, we forced the FLOR model with the Coupled Model Intercomparison Project Phase 6 (CMIP6) stratospheric aerosol dataset, starting from the first year of each initial condition, while keeping all other radiative forcing levels identical to those in the piControl simulation. The CMIP6 stratospheric aerosol dataset includes extinction coefficient, single scattering albedo and asymmetric factor for solar and terrestrial radiations, obtained by satellite observations²⁷ for the period of 1979–2014 and by AER-2D model²⁸ for volcanic eruption periods from 1850 to 1978. The latitudinal distribution of the extinction coefficient included in the CMIP6 stratospheric aerosol dataset, quantifying the weakness of radiation, shows distinct interhemispherical differences in aerosol plume distributions among the three volcanic eruptions (see fig. S1 of ref. 16). A detailed description of the CMIP6 stratospheric aerosol dataset for historical volcanic forcings is available at ftp://iacftp.ethz.ch/pub_read/luo/CMIP6/Readme_Data_Description.pdf. For each of the piControl (that is, non-eruption) and three tropical volcanic eruption simulations, we obtained 30 ensembles of monthly mean precipitation rate (kg m⁻² s⁻¹) and 2-m temperature (K) (that is, air temperature at 2 m above the ground) during the 5 years from the eruption year, which are used as input to the statistical flood model described in the following section. See ref. 16 for details on the experiment set-up.

Statistical flood model of seasonal peak flows

To predict seasonal peak flows under different volcanic forcings, we use the gauge-based statistical flood model developed in refs. 2,29, considering the seasonal maxima of mean daily discharges (used as an approximation of the instantaneous seasonal peak discharge) as the response variable and basin- and season-averaged precipitation and temperature as predictors. For each of the four seasons (that is, DJF, MAM, JJA and SON), this statistical relationship was established through a gamma regression model with three parameters: location (μ) and scale (σ), which control the median and dispersion of the gamma distribution, and the probability of zero occurrence (v), as described below:

$$\log(\mu) = \mu_0 + \mu_1 P_{\text{con}} + \mu_2 T_{\text{con}} + \mu_3 P_{\text{lag}} + \mu_4 T_{\text{lag}} \quad (1)$$

$$\log(\sigma) = \sigma_0 + \sigma_1 P_{\text{con}} + \sigma_2 T_{\text{con}} + \sigma_3 P_{\text{lag}} + \sigma_4 T_{\text{lag}} \quad (2)$$

$$\log\left(\frac{v}{1-v}\right) = v_0 + v_1 P_{\text{con}} + v_2 T_{\text{con}}, \quad (3)$$

where P_{con} (P_{lag}) and T_{con} (T_{lag}) are basin- and season-averaged monthly total precipitation (mm) and monthly mean temperature (°C) in the concurrent (previous) season of interest, respectively. Because this model provides a gamma distribution of peak flows for the season and year of interest, we can estimate the desired n -year RI peak flow based on the exceedance probability of the fitted distribution. Consequently, 7,886 streamgauges were chosen where a seasonal statistical flood model was developed on the basis of at least 30 years of observed

seasonal peak flows for all four seasons. When selecting the streamgauges, basin overlap was not considered. That is, for parent basins containing multiple nested basins, we included all streamgauges of both the parent and the nested basins. Streamgauges located within a polar region were also excluded.

As inputs to the statistical flood model, we convert monthly mean precipitation rate (kg m⁻² s⁻¹) and temperature (K) simulated from the FLOR model to season-averaged monthly total precipitation (mm) and monthly mean temperature (°C). We then calculate basin-average values for these season-averaged precipitation and temperature for each streamgauge's basin based on basin boundary shapes worldwide^{30,31}. Using these climate drivers as inputs to the statistical flood model, we generated 30 ensembles of seasonal peak flow series with various RIs under simulated global climates with three tropical volcanic eruptions and a non-eruption scenario, at each of the 7,886 streamgauges.

Detection of significant changes in seasonal peak flow induced by tropical volcanic eruptions

We use the Mann–Whitney U test^{32,33} to detect significant increasing (or decreasing) changes in seasonal peak flow induced by volcanic eruptions. The Mann–Whitney U test is a non-parametric test that is commonly used to compare whether there is a difference in two groups of non-normally distributed data. The null hypothesis for the test is that the two groups come from the same distribution. Therefore, whether the distribution of one group is greater (or smaller) than that of the other group can be tested using the one-sided test. The significance of peak flow change in each season between 30 ensemble members of the eruption and non-eruption simulations is determined using a one-sided Mann–Whitney U test at the 5% significance level.

To further investigate how many streamgauges are expected to show a significant change in peak flows by chance, we conduct additional resampling analysis based on a total of 60 ensemble members of simulated seasonal peak flows (that is, 30 members of eruption and another 30 members of non-eruption simulations) as follows:

- (1) For each streamgauge located within a given climate region and hemisphere, randomly divide the 60 ensemble members into 30 members of treatment and control groups.
- (2) Perform the Mann–Whitney U test to detect a significant increase (or decrease) in the treatment group relative to the control group.
- (3) Calculate the percentage of streamgauges with a statistically significant increase (or decrease) at the 5% significance level.
- (4) Repeat (1)–(3) 1,000 times, and obtain the upper 5th percentile of the resulting distribution of percentages

The upper 5th percentile value is used as the threshold percentage above which the percentage of streamgauges showing a significant increase (or decrease) is not due to chance at the 5% significance level.

Definition of climate regions based on Köppen–Geiger classification map

To assess whether there are differences in the patterns of peak flow responses to volcanic eruptions depending on climate regions, we classify 7,886 streamgauges into four climate types (that is, tropical, arid, temperate and cold) based on the present-day Köppen–Geiger climate classification map with a high spatial resolution (~0.083°)³⁴ (Extended Data Fig. 1). For each basin boundary, we count the number of pixels corresponding to each climate type and determine the type with the most pixels as the representative climate type. We exclude the cold region in the SH owing to the insufficient number of streamgauges in that region.

Selection of streamgauges with non-overlapping basins

To assess the impact of overlapping basins on our analysis, we identify the streamgauges with non-overlapping basins by screening out those

with nested basins. If we consider only the streamgauges of parent basins (that is, at the lowest downstream location), many streamgauges located within large parent basins (for example, Mississippi River Basin) cannot be available. To select as many streamgauges with non-overlapping basins as possible, we set a basin size threshold and consider streamgauges of parent basins only among those stations with basin sizes smaller than the threshold. For streamgauges with basin sizes larger than a given threshold, only those that have no other streamgauges within their basins are considered. We finally selected 4,886 streamgauges with non-overlapping basins using a basin size threshold of 158.5 km^2 , representing the largest number of non-overlapping streamgauges achievable across all tested basin-size thresholds (Extended Data Fig. 2).

Flood magnitude changes due to tropical volcanic eruptions

To quantify changes in flood magnitude caused by tropical volcanic eruptions, we first calculate the median seasonal peak flow from 30 ensemble members of simulations at each streamgauge. We then calculate the percentage change in ensemble median of seasonal peak flows as follows:

$$\Delta Q_{\text{ens.med}}^{n\text{-year}} = Q_{\text{volc}}^{n\text{-year}} - Q_{\text{ref}}^{n\text{-year}} \quad (4)$$

$$r\Delta Q_{\text{ens.med}}^{n\text{-year}} = \Delta Q_{\text{ens.med}}^{n\text{-year}} / Q_{\text{ref}}^{n\text{-year}} \times 100(\%), \quad (5)$$

where $Q_{\text{volc}}^{n\text{-year}}$ and $Q_{\text{ref}}^{n\text{-year}}$ are the ensemble median of n -year RI discharge from eruption and non-eruption simulations, respectively. We examine these changes at the regional scale by calculating their median across streamgauges, stratified by hemisphere, climate region and the sign of the changes.

Data availability

The worldwide basin boundary data for 7,886 streamgauges are obtained from different streamflow databases: African Database of Hydrometric Indices (ADHI) for Africa (available at <https://doi.org/10.23708/LXGXQ9>), Australian Bureau of Meteorology's Hydrologic Reference Stations (HRS) for Australia (available at <http://www.bom.gov.au/water/hrs/>), United States Geological Survey Streamgage NHDPlus Version 1 basins 2011 for conterminous United States (available at https://water.usgs.gov/lookup/getspatial?streamgage_basins) and Global Streamflow Indices and Metadata archive (GSIM) for the others (available at <https://doi.pangaea.de/10.1594/PANGAEA.887477>). The simulated seasonal peak flow datasets supporting the findings of this study are available via Zenodo at <https://doi.org/10.5281/zenodo.1603786> (ref. 35). Source data are provided with this paper.

Code availability

Codes that were used in this study are available upon request to the corresponding author.

References

27. Thomason, L. W. et al. A global space-based stratospheric aerosol climatology: 1979–2016. *Earth Syst. Sci. Data* **10**, 469–492 (2018).
28. Arfeuille, F. et al. Volcanic forcing for climate modeling: a new microphysics-based data set covering years 1600–present. *Clim. Past* **10**, 359–375 (2014).
29. Kim, H. & Villarini, G. On the attribution of annual maximum discharge across the conterminous United States. *Adv. Water Resour.* **171**, 104360 (2023).
30. Do, H. X., Gudmundsson, L., Leonard, M. & Westra, S. The Global Streamflow Indices and Metadata Archive (GSIM)-Part 1: the production of a daily streamflow archive and metadata. *Earth Syst. Sci. Data* **10**, 765–785 (2018).
31. Tramblay, Y. et al. ADHI: the African Database of Hydrometric Indices (1950–2018). *Earth Syst. Sci. Data* **13**, 1547–1560 (2021).
32. Mann, H. B. & Whitney, D. R. On a test of whether one of two random variables is stochastically larger than the other. *Ann. Math. Stat.* **18**, 50–60 (1947).
33. Wilcoxon, F. Individual comparisons by ranking methods. *Biometr. Bull.* **1**, 80–83 (1945).
34. Beck, H. E. et al. Present and future Köppen–Geiger climate classification maps at 1-km resolution. *Sci. Data* **5**, 180214 (2018).
35. Kim, H. Global response of floods to tropical explosive volcanic eruptions. Zenodo <https://doi.org/10.5281/zenodo.1603786> (2025).

Acknowledgements

The research was supported in part by funding provided by Princeton University.

Author contributions

H.K. processed the data, conducted the analyses, created the figures, interpreted the results and prepared the paper. G. Villarini designed the study, interpreted the results and prepared the paper. W.Y. processed the data, interpreted the results and prepared the paper. G. Vecchi interpreted the results and prepared the paper. All authors reviewed and edited the final version of the paper.

Competing interests

The authors declare no competing interests.

Additional information

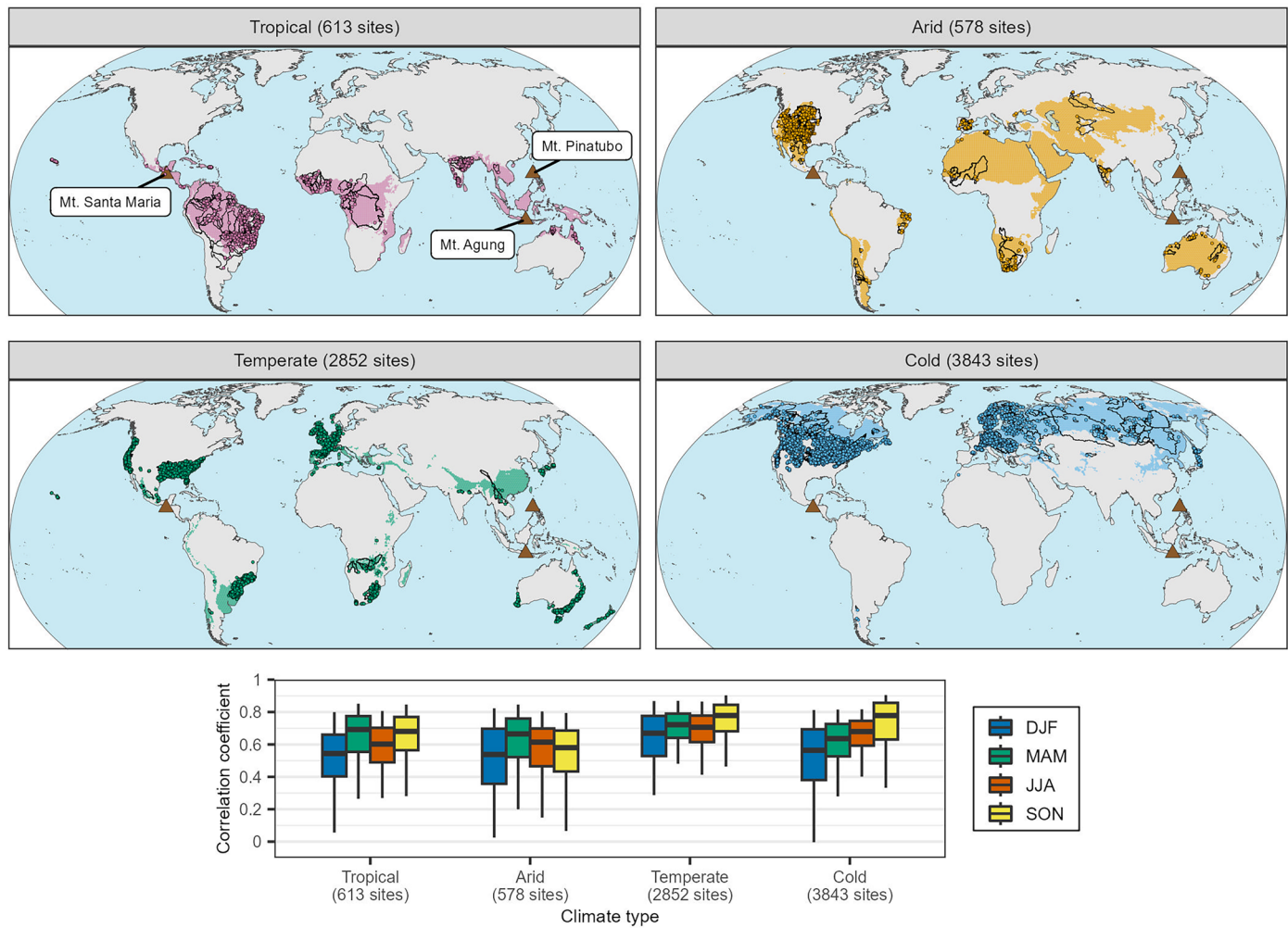
Extended data is available for this paper at <https://doi.org/10.1038/s41561-025-01782-5>.

Supplementary information The online version contains supplementary material available at <https://doi.org/10.1038/s41561-025-01782-5>.

Correspondence and requests for materials should be addressed to Gabriele Villarini.

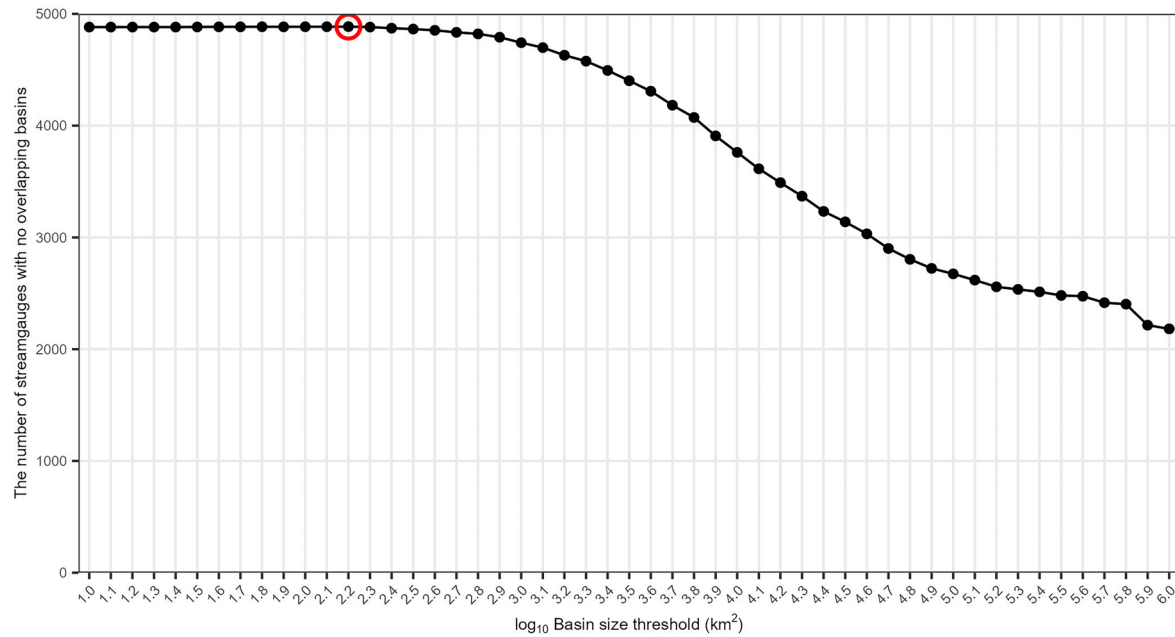
Peer review information *Nature Geoscience* thanks Jon Major and the other, anonymous, reviewer(s) for their contribution to the peer review of this work. Primary Handling Editor: Tamara Goldin, in collaboration with the *Nature Geoscience* team.

Reprints and permissions information is available at www.nature.com/reprints.

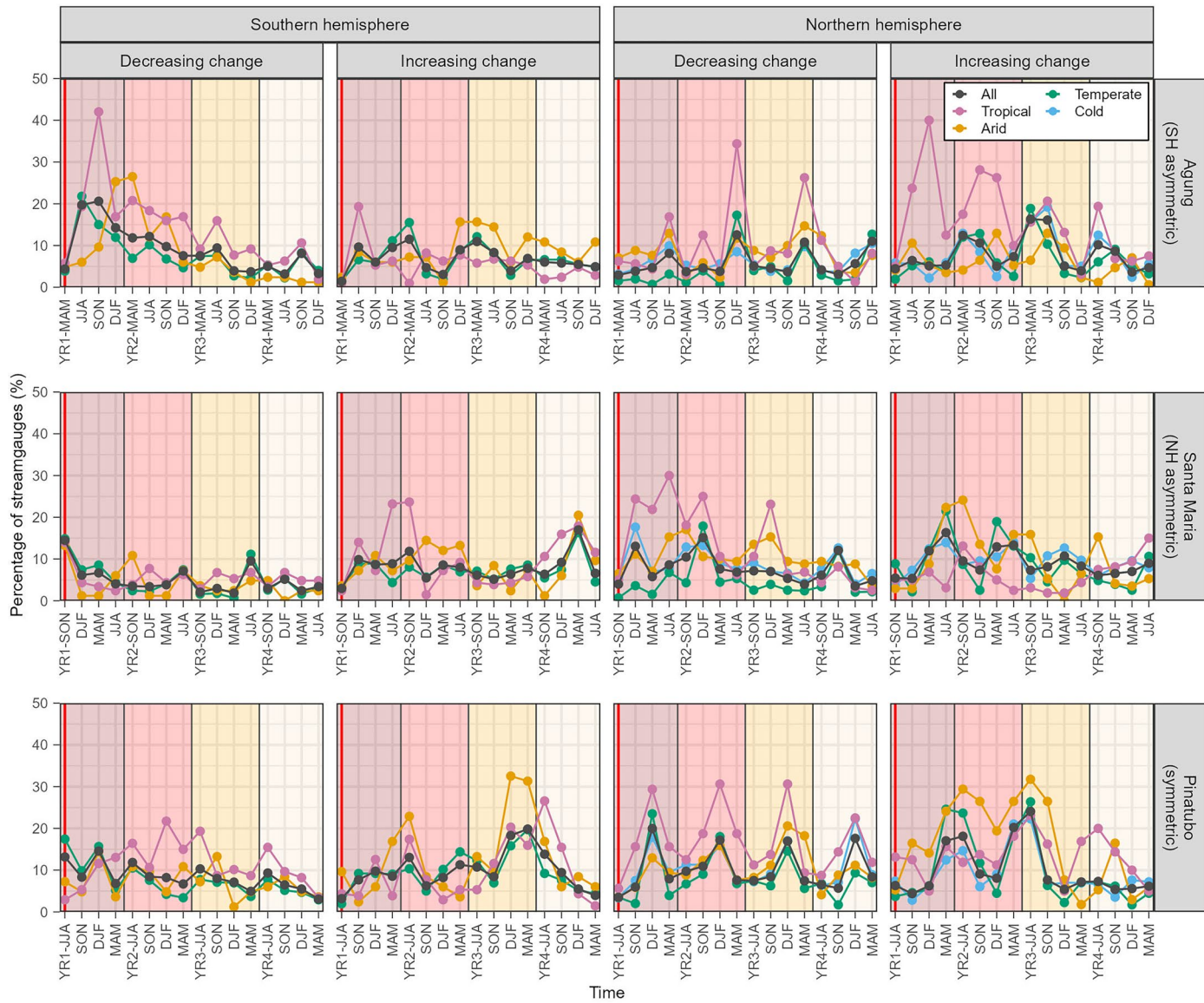


Extended Data Fig. 1 | Maps showing the location of three volcanoes (triangles) and streamgauges used in this study. The numbers in parentheses in the titles of the top and middle panels and on the x-axis of the bottom panel represent the number of streamgauges within each climate region. Basin boundaries are shown with bold lines. Colored pixels on land indicate the corresponding climate

regions. The boxplots (bottom panel) show the distribution of correlation coefficients between observed and modeled seasonal peak flows across streamgauges stratified by four climate types. In the boxplot, the limits of the box (whiskers) represent the 25th and 75th (5th and 95th) percentiles, while the line inside of the box indicates the median. Figure modified from ref. 2.



Extended Data Fig. 2 | Sensitivity of the number of streamgauges with no overlapping basins to the basin size thresholds. The point with red circle indicates the maximum number of streamgauges with no overlapping basins which is finally selected to assess the impact of overlapping basins on prevalence of flood responses.

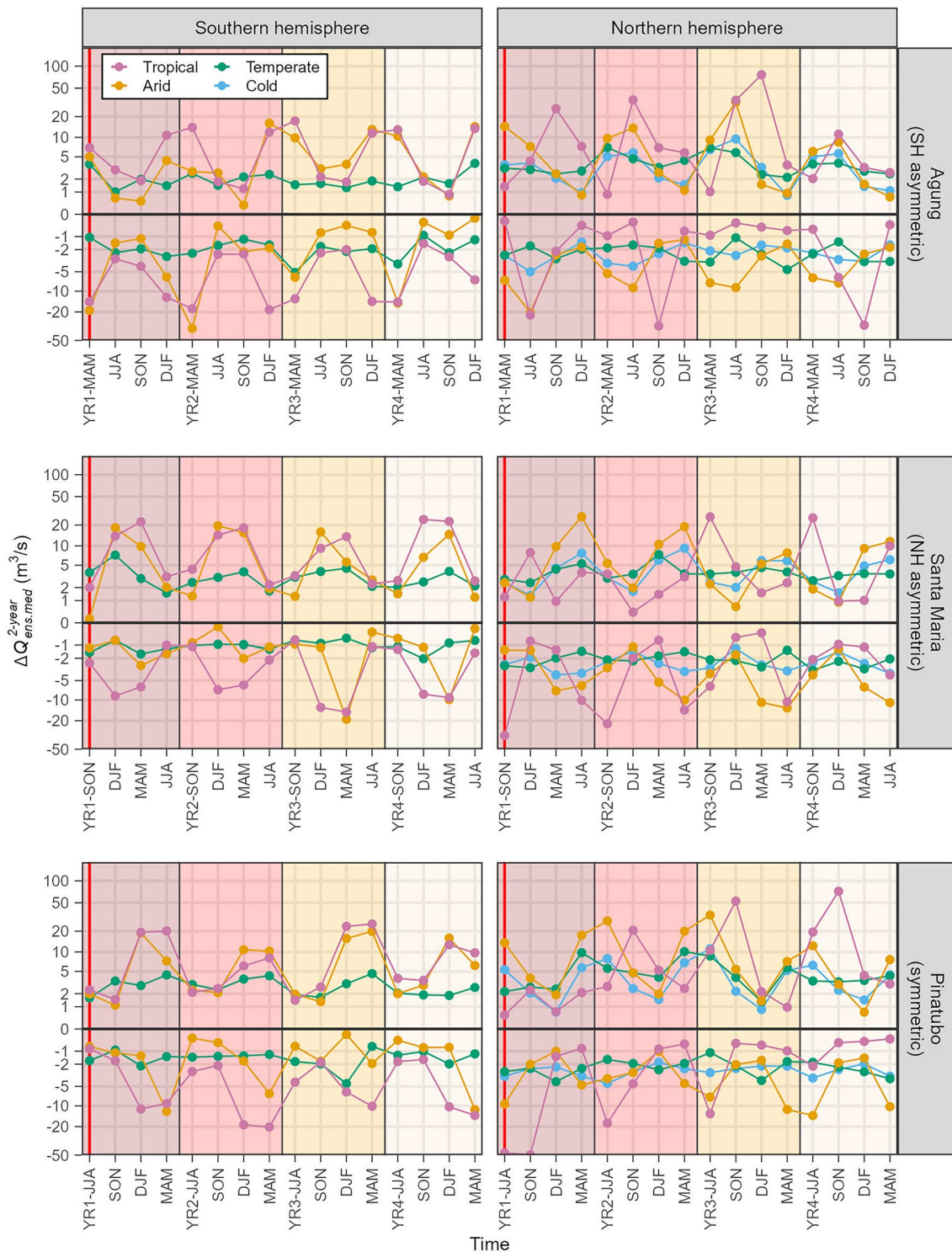


Extended Data Fig. 3 | Changes over time in the prevalence of the 2-year return interval discharges in response to tropical volcanic eruptions. Same as Fig. 1 in the main text, but for 4,886 streamgauges with non-overlapping basins only.



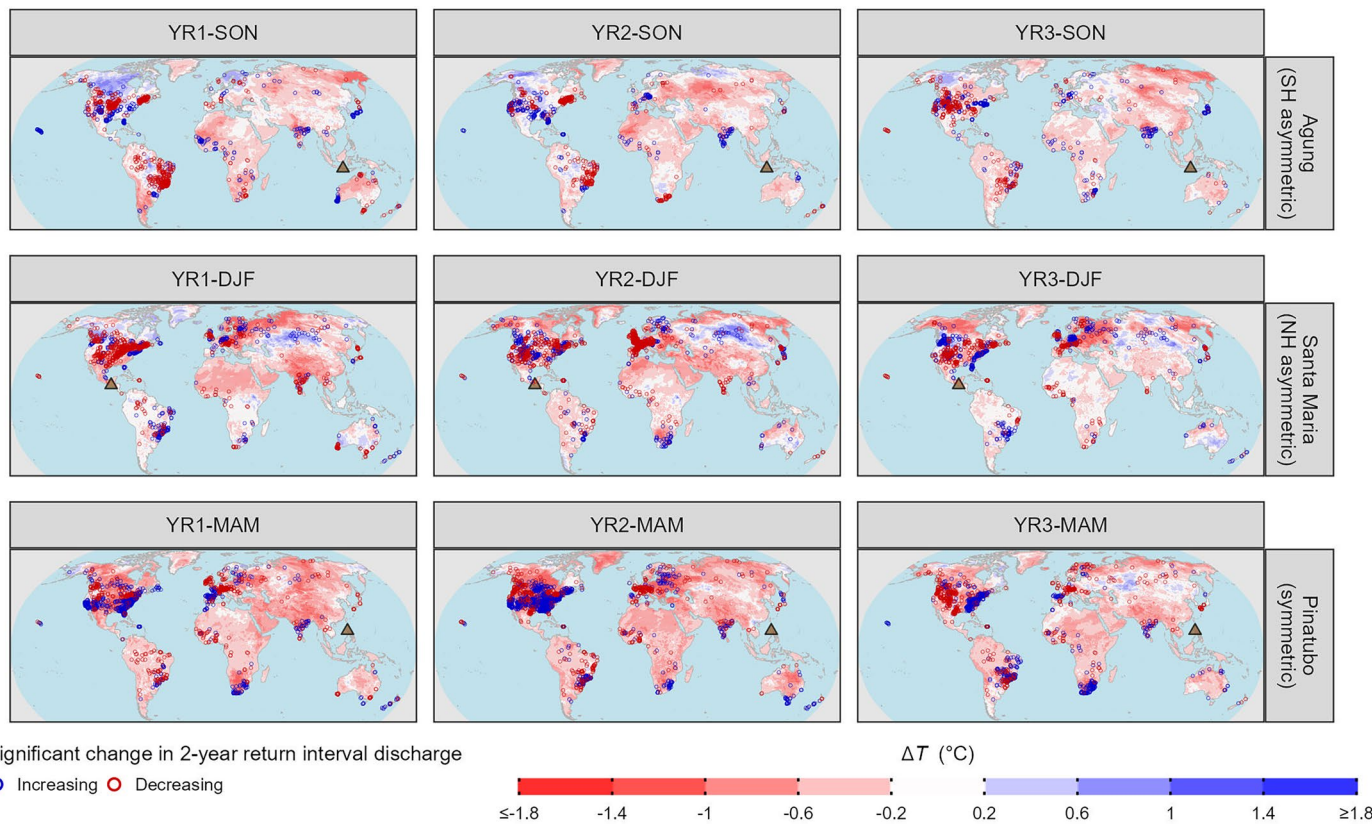
Extended Data Fig. 4 | Changes over time in the prevalence of the 2-year return interval discharges in response to tropical volcanic eruptions. Same as Fig. 1 in the main text, but for: **a**) 6,336 streamgauges whose statistical flood models show a correlation coefficient of at least 0.3 between observed and modeled peak flows

for all four seasons; and **b**) 4,193 streamgauges whose statistical flood models show a correlation coefficient of at least 0.5 between observed and modeled peak flows for all four seasons.



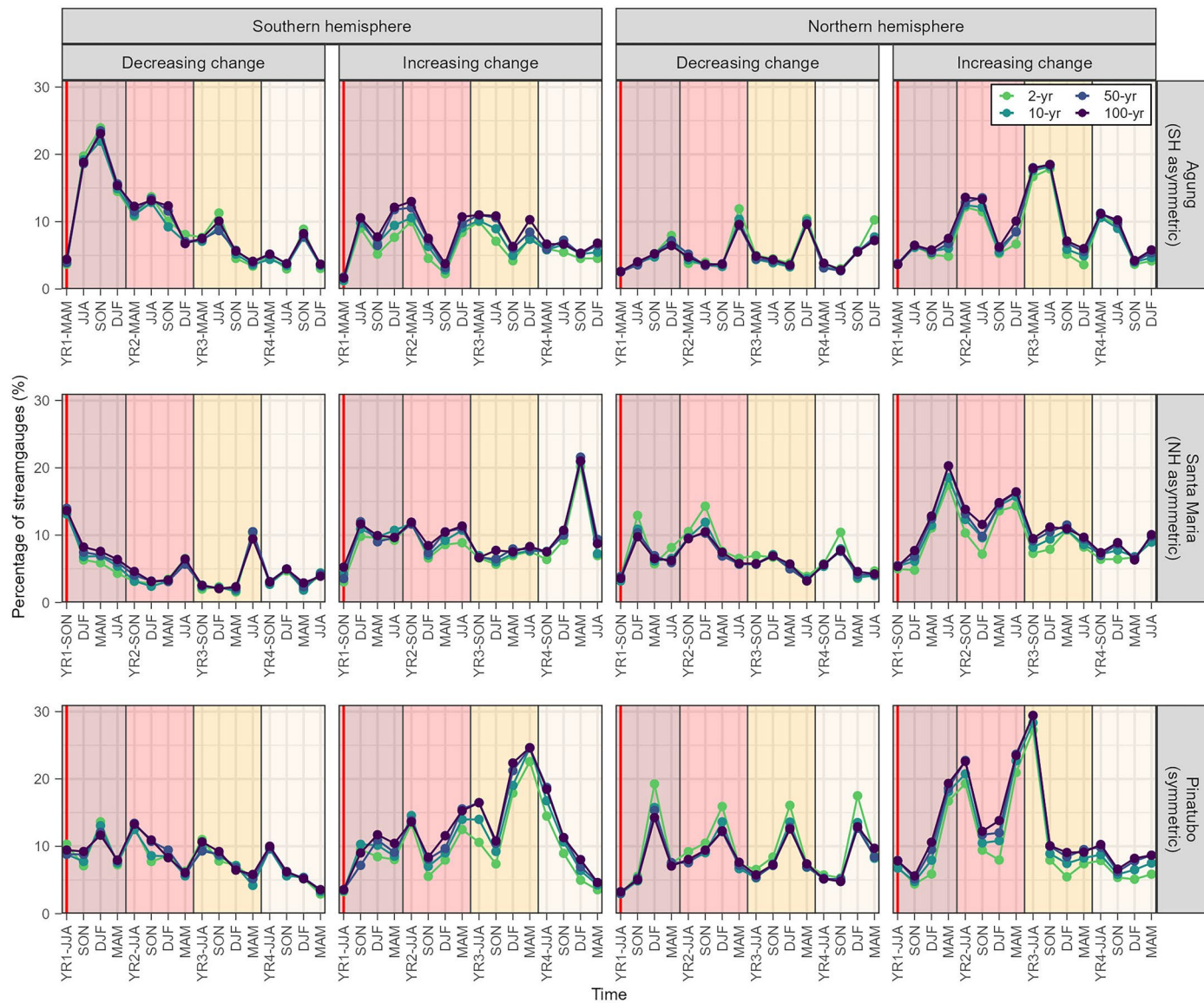
Extended Data Fig. 5 | Changes over time in the regional average of the absolute changes in the magnitude of the 2-year return interval discharges in response to tropical volcanic eruptions. Changes in the discharge magnitude due to the eruptions are calculated by subtracting the ensemble median of 30 non-eruption simulations from that of 30 eruption simulations. The regional average values are then obtained by taking the median across the streamgauges stratified by tropical (magenta line), arid (orange line), temperate (green

line), and cold (light blue line) regions. The lines above (below) zero show the results for streamgauges experiencing increasing (decreasing) discharge due to eruptions. The vertical red line indicates the season in which the eruption occurred. The shaded areas separated by different colors and vertical black lines represent each year, from the first (YR1) to the fourth year (YR4) after the eruption. Panels show results for Agung (Indonesia), Santa Maria (Guatemala), and Pinatubo (Philippines) eruptions.



Extended Data Fig. 6 | Global responses of the 2-year return interval discharges and seasonal temperature to tropical volcanic eruptions. The red (blue) circles show the streamgauges having statistically significant decrease (increase) in the 2-year return interval discharge due to the eruptions. Grid cells inland indicate absolute change in the median of the season-averaged temperatures across 30 ensemble members. The redder grids represent greater

decreases, while the bluer grids represent greater increases in temperature due to the eruptions. Three rows represent the results for September-November season for Agung (Indonesia), December-February season for Santa María (Guatemala), and March-May season for Pinatubo (Philippines) eruptions, from top to bottom. Three columns represent the results of the first (YR1), second (YR2), and third year (YR3) after eruptions, from left to right.



Extended Data Fig. 7 | Responses of discharges for different return intervals to tropical volcanic eruptions. Percentages of streamgauges showing significant decreases (first and third columns) and increases (second and fourth columns) in peak discharges calculated for 2-, 10-, 50-, and 100-year return intervals. The darker the color, the greater the discharge return interval. The vertical red line

indicates the season in which the eruption occurred. The shaded areas separated by different colors and vertical black lines represent each year, from the first (YR1) to the fourth year (YR4) after the eruption. Panels show results for Agung (Indonesia), Santa María (Guatemala), and Pinatubo (Philippines) eruptions.